Article

Mathematical Modeling and Validation of Glucose Compensation of the *Neurospora* Circadian Clock

Andrey A. Dovzhenok,[1] Mokryun Baek,[2] Sookkyung Lim,[1] and Christian I. Hong[2,*]
[1]Department of Mathematical Sciences, University of Cincinnati, Cincinnati, Ohio; and [2]Department of Molecular and Cellular Physiology, University of Cincinnati College of Medicine, Cincinnati, Ohio

ABSTRACT Autonomous circadian oscillations arise from transcriptional-translational feedback loops of core clock components. The period of a circadian oscillator is relatively insensitive to changes in nutrients (e.g., glucose), which is referred to as "nutrient compensation". Recently, a transcription repressor, CSP-1, was identified as a component of the circadian system in *Neurospora crassa*. The transcription of *csp-1* is under the circadian regulation. Intriguingly, CSP-1 represses the circadian transcription factor, WC-1, forming a negative feedback loop that can influence the core oscillator. This feedback mechanism is suggested to maintain the circadian period in a wide range of glucose concentrations. In this report, we constructed a mathematical model of the *Neurospora* circadian clock incorporating the above WC-1/CSP-1 feedback loop, and investigated molecular mechanisms of glucose compensation. Our model shows that glucose compensation exists within a narrow range of parameter space where the activation rates of *csp-1* and *wc-1* are balanced with each other, and simulates loss of glucose compensation in *csp-1* mutants. More importantly, we experimentally validated rhythmic oscillations of the *wc-1* gene expression and loss of glucose compensation in the $wc\text{-}1^{ov}$ mutant as predicted in the model. Furthermore, our stochastic simulations demonstrate that the CSP-1-dependent negative feedback loop functions in glucose compensation, but does not enhance the overall robustness of oscillations against molecular noise. Our work highlights predictive modeling of circadian clock machinery and experimental validations employing *Neurospora* and brings a deeper understanding of molecular mechanisms of glucose compensation.

INTRODUCTION

Circadian rhythms play a vital role in an organism's functions by anticipating daily changes in its environment. They influence various facets of organisms' activity including physiology, cell cycle, and metabolism. In the last two decades, experiments revealed that the core clock components used to construct the circadian oscillator are assembled as transcription-translation feedback loops (1,2) whose activity is modified through posttranslational modifications of the core components (3,4).

In *Neurospora crassa*, circadian timekeeping is sustained through interlocked negative and positive feedback loops. The WHITE COLLAR complex (WCC), a heterodimer of the zinc-finger proteins WC-1 and WC-2, activates the transcription of the *frequency* (*frq*) gene (5–7). Then, translated FREQUENCY (FRQ) protein binds to FRQ-interacting RNA Helicase and CK1 (3,8), translocates into the nucleus, and suppresses its own transcription by inactivating WCC, closing the negative feedback loop (9–11). Simultaneously, FRQ promotes WC-1 accumulation in the cytoplasm, increasing the level of WCC forming a positive feedback loop (12,13).

Recently, the circadian clock-regulated developmental regulator, *conidial separation-1* (*csp-1*) (14), was shown to be a global transcription repressor under the direct control of WCC, and was found to regulate expression of various metabolic and other genes (15). CSP-1 was shown to repress the expression of *wc-1* in a glucose-dependent manner by binding at the respective promoter (16) and forming an additional negative feedback loop. These intriguing findings illuminate a novel function of CSP-1 as an important regulator of the *Neurospora* core clock oscillator resembling that of REV-ERB-α/β in the mammalian circadian clock (17–19). Further experiments suggested that negative feedback via CSP-1 maintains relatively similar abundance of WC-1 in a wide range of glucose concentrations in the growth media. This results in a relatively constant circadian period as a function of glucose concentrations, which is referred to as "glucose compensation". In contrast, the glucose compensation was disrupted in $csp\text{-}1^{ko}$ with decreasing period with increasing glucose concentration (16).

In this article, we explore a *Neurospora* circadian clock model that includes CSP-1 as a newly identified element of the circadian system, and investigate molecular mechanisms for glucose compensation. Our model simulates glucose compensation of period by balancing the activation rates of *csp-1* and *wc-1* transcription, and loss of glucose

Submitted September 12, 2014, and accepted for publication January 9, 2015.

*Correspondence: christian.hong@uc.edu

Editor: James Keener.

0006-3495/15/04/1830/10 $2.00

http://dx.doi.org/10.1016/j.bpj.2015.01.043

compensation in *csp-1* mutants. Moreover, we predict and experimentally validate loss of glucose compensation in the *wc-1* overexpression (*wc-1*^{ov}) mutant. The model also accurately reproduces changes in clock period observed in previous experiments, and differential expression of FRQ and WC-1 in the nucleus versus cytoplasm (4,20).

Finally, it has been shown that the interlocked dual negative feedback loop increases oscillatory domain and possibly enhances the robustness of autonomous oscillations (21). We investigate robustness of the system against molecular stochasticity in the presence or absence of CSP-1 and show that a CSP-1-mediated negative feedback loop does not enhance the overall robustness of the system against molecular noise.

MATERIALS AND METHODS

Mathematical model of *Neurospora* circadian clock with CSP-1

The wiring diagram of the core oscillator and other ancillary components pertinent to this discussion is shown in Fig. 1. In the nucleus, nuclear WC-1 (WC-1$_n$) activates *frq* transcription with the rate constant k_1. FRQ protein is translated from *frq* mRNA in the cytosol and is translocated into the nucleus (processes with the rate constants k_2 and k_3, respectively). *frq* mRNA, cytosolic FRQ (FRQ$_c$), and nuclear FRQ (FRQ$_n$) degrade with the rate constants k_4, k_5, and k_6, respectively. The expression of *wc-1* is modeled with a maximum rate constant k_7, and the *wc-1* expression is modulated by the negative feedback from the global transcription repressor, CSP-1. Cytosolic WC-1 (WC-1$_c$) is translated and degraded with the rate constants k_8 and k_{10}, respectively. We assume that the accumulation of WC-1$_c$ is positively regulated by FRQ$_c$ (12). Then, WC-1$_c$ protein is either degraded (k_{11}) or translocated into the nucleus (k_9). We do not consider WC-2 in the model because WC-2 is present in excess of WC-1 and its concentration is relatively constant at all circadian times (6,7). Therefore, we consider the WCC complex to be represented in the model by WC-1$_n$. Finally, WC-1$_n$ starts *frq* transcription and then either slowly degrades (k_{12}) or is quickly inactivated (k_{13}/k_{14}) and degraded (k_{15}) via complex-formation with FRQ$_n$ closing the negative feedback loop.

Based on recent experimental findings (15,16), we extended the *Neurospora* circadian clock model (22) to include an additional negative feedback loop formed by the aforementioned transcriptional repressor, CSP-1. WC-1$_n$ starts transcription of *csp-1* (k_{16}), and the *csp-1* mRNA is degraded with the rate k_{17}. CSP-1 is translated and degraded with the rates k_{18} and k_{19}, respectively. We used the rate of degradation of CSP-1 from the previous experimental measurements (15). In the nucleus, CSP-1 inhibits the expression of *wc-1* as well as its own expression, as reported in Sancar et al. (15). In this study, we assume that the binding of CSP-1 to the *wc-1* promoter can be described by the Hill-type function similar to the one used to model inhibition of its own transcription in Sancar et al. (15).

The model includes the following rate equations:

$$\frac{d[frq\ \ \mathrm{mRNA}]}{dt} = k_1\frac{[\mathrm{WC\text{-}1_n}]^6}{K+[\mathrm{WC\text{-}1_n}]^6} - k_4[frq\ \ \mathrm{mRNA}] + k_{01},$$

$$\frac{d[\mathrm{FRQ_c}]}{dt} = k_2[frq\ \ \mathrm{mRNA}] - (k_3+k_5)[\mathrm{FRQ_c}],$$

$$\frac{d[\mathrm{FRQ_n}]}{dt} = k_3[\mathrm{FRQ_c}] + k_{14}[\mathrm{FRQ_n : WC\text{-}1_n}] - [\mathrm{FRQ_n}](k_6 + k_{13}[\mathrm{WC\text{-}1_n}]),$$

$$\frac{d[wc\text{-}1\ \ \mathrm{mRNA}]}{dt} = k_7\frac{K_1}{K_1+[\mathrm{CSP\text{-}1}]} - k_{10}[wc\text{-}1\ \ \mathrm{mRNA}] + k_{03},$$

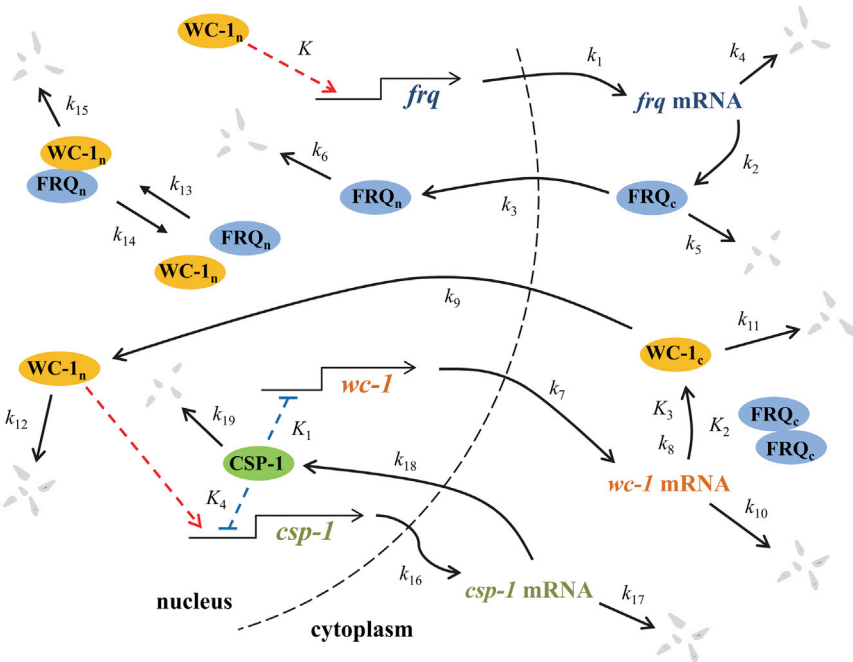

FIGURE 1 *Neurospora* clock model diagram with the global transcription repressor CSP-1. Transcriptional activator WC-1 starts transcription of the core clock gene *frq* whereas FRQ protein represses its own gene transcription in a negative feedback loop that promotes sustained circadian oscillations of core clock proteins. Transcriptional repressor CSP-1 inhibits *wc-1* gene expression forming another negative feedback loop in the model. (*Dashed arrows*) Activation, (*dashed lines* with *blunt ends*) repression via binding at the respective promoters. To see this figure in color, go online.

$$\frac{d[\text{WC-1}_\text{c}]}{dt} = k_8\frac{[\text{FRQ}_\text{c}]^2}{K_2+[\text{FRQ}_\text{c}]^2}\frac{[wc\text{-}1\ \ \text{mRNA}]}{K_3+[wc\text{-}1\ \ \text{mRNA}]} - (k_9+k_{11})[\text{WC}\ \ \text{-1}_\text{c}],$$

$$\frac{d[\text{WC-1}_\text{n}]}{dt} = k_9[\text{WC-1}_\text{c}] - [\text{WC-1}_\text{n}](k_{12}+k_{13}[\text{FRQ}_\text{n}]) + k_{14}[\text{FRQ}_\text{n}\text{: WC-1}_\text{n}],$$

$$\frac{d[\text{FRQ}_\text{n}\text{: WC-1}_\text{n}]}{dt} = k_{13}[\text{FRQ}_\text{n}]\times[\text{WC-1}_\text{n}] - (k_{14}+k_{15})[\text{FRQ}_\text{n}\text{: WC-1}_\text{n}],$$

$$\frac{d[csp\text{-}1\ \ \text{mRNA}]}{dt} = k_{16}[\text{WC-1}_\text{n}]\frac{K_4}{K_4+[\text{CSP-1}]} - k_{17}[csp\text{-}1\ \ \text{mRNA}]+k_{04},$$

$$\frac{d[\text{CSP-1}]}{dt} = k_{18}[csp\text{-}1\ \ \text{mRNA}]-k_{19}[\text{CSP-1}].$$

The parameter values are given in Table 1 (23–25). Parameters k_{01}, k_{03}, and k_{04} simulate additional transcription of corresponding genes to reproduce overexpression experiments with an inducible system, and have dimensions of a.u. h^{-1} and are initially set to zero. Concentrations in arbitrary units (a.u.) reflect the number of molecules per unit volume. Experimentally measured rate constants are indicated in Table 1. The rest of the rate constants have been chosen to fit the model to experimental data simulating the abundance of total and nuclear WC-1 and FRQ, and the period change observed in *frq*, *wc-1*, and *csp-1* overexpression experiments in wild-type (WT) and mutant strains.

Justifications of the model

In this study, we use a relatively high cooperativity ($n = 6$) of WC-1_n binding at the *frq* promoter. This high cooperativity is necessary to increase nonlinearity in our simple model to simulate the existing experimental data on changes in period in clock overexpression mutants (see Fig. 3 and Text S1 in the Supporting Material for more details). In our model, we do not include posttranslational modification such as progressive phosphorylation of FRQ (26) or the coiled-coil domain-mediated FRQ-FRQ interaction (4) to reduce the complexity of the model while simulating existing molecular phenotypes. If they are included in the model, they may increase overall nonlinearity of the system and allow for a lower Hill coefficient of WC-1_n activation of *frq* transcription. However, this would make the model significantly more complex and, therefore, we do not include them in this simple model. See also Text S1 in the Supporting Material for further discussion. Also, we assume that the accumulation of WC-1_c shows saturation kinetics with reference to *wc-1* mRNA. This saturation behavior, although not reported experimentally, may occur due to FRQ-promoted accumulation of WC-1_c as we showed before in Hong et al. (22) and allows the model to reproduce experimental data on *wc-1* overexpression (see Fig. 3, *B* and *C* and Text S1 for more details).

Lastly, in our stochastic simulations, we used standard Michaelis-Menten and Hill-type functions (Table S1 in the Supporting Material) derived via quasi-steady-state approximation instead of a large number of elementary reactions. This approach, resulting in a compact model description, was studied before in a circadian clock model (27) and other systems (28) and was shown to produce satisfactory agreement between detailed and compact models. The compact models are favorable because the actual molecular mechanisms that comprise Hill-type and Michaelis-Menten functions are usually unknown. However, recent studies have found that stochastic simulations of the compact model are not always accurate (29–31). We confirm validity of our stochastic simulation results produced with the Gillespie algorithm by rewriting the model as Langevin-type equations with additive or multiplicative noise (32) and obtaining qualitatively similar results (see Figs. 7 and S9).

TABLE 1 Parameter values for the *Neurospora* clock model

Parameter	Value	Dimension	Parameter	Value	Dimension
k_1	1.8	a.u. h^{-1}	k_{13}	50	$(\text{a.u.})^{-1}\ h^{-1}$
k_2	1.8	h^{-1}	k_{14}	1	h^{-1}
k_3	0.05	h^{-1}	k_{15}	5	h^{-1}
k_4 (23)	0.23	h^{-1}	k_{16}	0.12	h^{-1}
k_5 (24)	0.27	h^{-1}	k_{17}	1.4	h^{-1}
k_6 (24)	0.27	h^{-1}	k_{18}	50	h^{-1}
k_7	0.5	a.u. h^{-1}	k_{19} (15)	1.4	h^{-1}
k_8	1	a.u. h^{-1}	K	1.25	$(\text{a.u.})^6$
k_9	40	h^{-1}	K_1	3	a.u.
k_{10} (25)	0.1	h^{-1}	K_2	1	$(\text{a.u.})^2$
k_{11}	0.05	h^{-1}	K_3	10	a.u.
k_{12}	0.02	h^{-1}	K_4	3	a.u.

Experimentally measured rate constants are followed by a reference.

Computer simulations

We used XPPAUT software (Bard Ermentrout, University of Pittsburgh, http://www.math.pitt.edu/bard/xpp/xpp.html) to obtain numerical solutions, bifurcation, and period diagrams of the model equations.

Stochastic simulations

Stochastic simulations were carried out in MATLAB (The MathWorks, Natick, MA) by utilizing the Gillespie algorithm (33,34). We assigned the probability of occurrence of a particular reaction to each term of the kinetic model as shown in Table S1. The Gillespie algorithm then randomly chooses the reaction that occurs at each time step according to its probability and the time interval to the next reaction step. The number of molecules and the reaction probabilities are then updated at each time step according to Table S1. Parameter Ω in the Gillespie method allows modulation of the strength of noise in the stochastic model formulation by controlling the number of molecules that are present in the system. Each simulation was run for 3000 h and we removed the first 500 h to allow for transients to subside.

Strains

Strains used for the experiments are a clock wild-type *ras-1*^{bd} (328-4), *wc-1-luc::csr-1*, and *wc-1*^{ov};*frq-luc::his-3*. The strain *wc-1-luc::csr-1* was created by integrating the *wc-1* promoter with a codon-optimized firefly luciferase into the *csr-1* locus as previously described in Chen et al. (35) in a clock wild-type *ras-1*^{bd} (328-4). The strain *wc-1*^{ov} was created by integrating a *wc-1* open reading frame with its endogenous promoter into the *csr-1* locus as previously described in Chen et al. (35) in the strain containing *frq-luciferase* reporter (36).

Western blot

Neurospora were grown in liquid culture media containing Vogel's medium (pH 5.8) with either 0.1% or 0.3% glucose, 0.5% arginine, 50 ng/mL biotin,

and harvested at indicated time points. Immunoblot analysis was performed as previously described in Garceau et al. (26) except that we used 1) 20 μg of protein per lane, 2) 6.5% sodium dodecyl sulfate-polyacrylamide gel electrophoresis, 3) anti-WC-1 or anti-FRQ (1:300) as primary antibody, and 4) goat anti-rabbit IgG (H+L) (1:5000, No. 170-6515; Bio-Rad, Hercules, CA) as secondary antibody.

Race tube and bioluminescence assays

Race tube and bioluminescence assays were performed as previously described in Hong et al. (37) and Dunlap and Loros (38). We used standard race tubes containing Vogel's medium (pH 5.8) with 0.17% arginine, 50 ng/mL biotin, 1.5% agar, and 12.5 μM of luciferin for bioluminescence assays, and varying concentrations of glucose (0.1–0.3% m/v).

RESULTS

The proposed circadian clock model reproduces wild-type and mutant phenotypes

Fig. 2, *A–C*, shows oscillation profiles derived from the simulated WT circadian system and Fig. 2 *D* shows experimental data from the *wc-1-luciferase* reporter.

The abundance of total FRQ is greater than the abundance of total WC-1 (20), and there is 4–10 h of phase difference between FRQ and WC-1 depending on whether we measure by the peak or trough of the protein concentrations (Fig. 2 *A*) (12). In contrast to total WC-1 and FRQ concentrations, $WC\text{-}1_n$ levels are higher than FRQ_n levels because FRQ is mainly localized in the cytoplasm (4,20), which is also simulated in our model (Fig. 2 *B*). Negative feedback from CSP-1 onto *wc-1* expression is moderate, resulting in low-amplitude oscillations of *wc-1* mRNA levels (Fig. 2 *C*) that were not reported previously. Oscillations of *wc-1* mRNA may not have been observed in previous experiments (12) due to their low amplitude and the presence of molecular noise. We constructed a *wc-1* bioluminescence reporter by fusing the promoter of *wc-1* with a codon-optimized firefly luciferase, and validated that gene expression of *wc-1* oscillates in a circadian manner (Fig. 2 *D*). Garceau et al. (26) observed a rapid rise in *frq* mRNA level and its subsequent rapid exponential decay. In contrast, the increase in FRQ protein concentration was followed by a slower, almost linear decay of FRQ protein level (26). In the model, the temporal profiles of *frq* mRNA (Fig. 2 *C*) and total FRQ protein (Fig. 2 *A*) accurately reproduce these distinct shapes of *frq* mRNA and FRQ protein oscillations. The expression of *csp-1* shows circadian oscillations with peak expression aligned with the peak of WC-1 (WCC) because its expression is controlled by WCC (14,15) (Fig. 2 *C*).

Our model not only reproduces wild-type profiles, but also simulates experimentally observed changes in period in different clock overexpression strains. In *Neurospora*, the quinic acid (QA)-inducible system is readily used to increase the expression of a target gene in a QA dosage-dependent manner (39,40). Use of this for *frq* overexpression (*frq*$^+$;*qa-2-frq*) results in small changes in period at low induction, and abolishes oscillations at high induction (40). In Fig. 3 *A*, we show that overexpression of *frq* with parameter k_{01} that simulates additional transcription of the *frq* gene (see model equations in Materials and Methods) does not produce large changes in period, and the system transitions into a stable steady state with no oscillations when the value of k_{01} is >0.14. It is important to note that

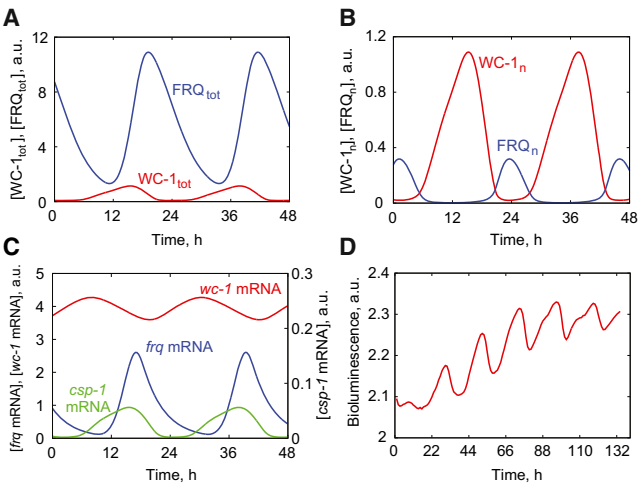

FIGURE 2 Oscillatory profiles for the wild-type parameterization. (*A*) Total WC-1 and FRQ levels show greater abundance of FRQ compared to WC-1. (*B*) The abundance of $WC\text{-}1_n$ is greater than FRQ_n for the most of circadian time. (*C*) All three transcripts of *frq*, *wc-1*, and *csp-1* show sustained oscillations. (*D*) The *wc-1-luciferase* reporter shows robust circadian oscillations as predicted in the model. This data is a representative of three independent experiments. Arbitrary units (a.u.) are shown. To see this figure in color, go online.

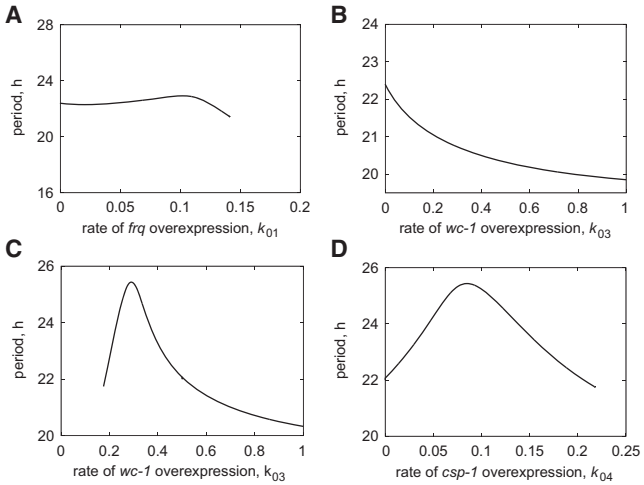

FIGURE 3 The model reproduces overexpression phenotypes of *frq*, *wc-1*, and *csp-1*. (*A*) Clock period as a function of the rate of *frq* overexpression, k_{01} in wild-type genetic background. (*B*) Clock period as a function of *wc-1* overexpression rate, k_{03}, in wild-type genetic background. (*C*) Clock period as a function of *wc-1* overexpression rate, k_{03}, in *wc-1*^{ko} genetic background (the *wc-1* expression rate constant $k_7 = 0$). (*D*) Clock period as a function of k_{04}, simulating the rate of *csp-1* overexpression in *qa-2* promoter knock-in experiment (the *csp-1* expression rate constant $k_{16} = 0$).

the amplitude of FRQ_n plays a critical role in determining the period of the system (Fig. S1 in the Supporting Material). The period is maintained in the case of *frq* overexpression, because there is only a minimal change in the amplitude of FRQ_n oscillations before the system transitions to a stable steady state crossing a Hopf bifurcation point (Fig. S2).

On the other hand, *wc-1* overexpression (*wc-1*$^+$;*qa-2-wc-1*) experiments reveal a monotonically decreasing period with increasing concentration of the inducer, QA (6). This decrease of period is observed as a function of the rate of *wc-1* overexpression, k_{03} (Fig. 3 *B*). Cheng et al. (6) also performed overexpression of *wc-1* in the *wc-1*^{ko} background (*wc-1*^{ko};*qa-2-wc-1*), and observed no oscillations at low QA levels. However, the period decreased from ~24.5 h to 22.8 h at higher QA levels (6). Our model reproduces experimentally observed shortening of the period with the increase in *wc-1* overexpression rate k_{03} in a simulated *wc-1*^{ko} strain ($k_7 = 0$) (Fig. 3 *C*). The initial transient increase of the period in the model (Fig. 3 *C*) corresponds to the parameter range near the Hopf bifurcation that is characterized by low albeit increasing amplitude of FRQ_n oscillations (Fig. S3 and see Text S2 in the Supporting Material for the mechanism of period regulation), which are easily destroyed in the model in the presence of molecular noise (Fig. S4).

In contrast to the decrease of period with *wc-1* overexpression, Sancar et al. (15) observed an increase of period by ~2.5 h with a moderate overexpression of *csp-1*, and then a loss of circadian rhythms with higher induction of *csp-1* in a *csp-1*^{ko} background (*csp-1*^{ko};*qa-2-csp-1*) (15). Our model reproduces period lengthening of the circadian clock with the increase of *csp-1* expression as modeled by increasing the rate of *csp-1* overexpression, k_{04}, in the *csp-1*^{ko} background ($k_{16} = 0$) (Fig. 3 *D*). The increase of period coincides with the rapid decrease in FRQ_n levels (Fig. S5, *A* and *B*, and see Text S2 in the Supporting Material). Interestingly, FRQ_c levels decrease more gradually than FRQ_n (Fig. S5 *B*). Finally, a decrease in period occurs in the model for larger values of k_{04} (Fig. 3 *D*). This period decrease is characterized by low abundance of FRQ_n (Fig. S5 *B*) that is no longer able to effectively clear WC-1 from the nucleus so that the amplitude of $WC\text{-}1_n$ oscillations becomes small (Fig. S5 *C*). These low-amplitude oscillations are likely to be destroyed by molecular noise (see Fig. S4) and, therefore, may not be observed experimentally (16). This conclusion is indirectly suggested by a strongly damped amplitude of *frq-luc* bioluminescence as well as weakened conidiation rhythm observed at an intermediate QA level right before the loss of circadian oscillations in *csp-1* overexpression experiments (16). It is important to note that the increase in *csp-1* overexpression (k_{04}) corresponds to the decrease of *wc-1* overexpression rate, k_{03}, because of the repression CSP-1 exerts on *wc-1* transcription. Hence, the decrease of period observed in Fig. 3 *D* is equivalent to the increase of period shown in Fig. 3 *C*.

Point mutations of *frq* that alter the circadian period have been interpreted as changing the half-life of the FRQ protein (41,42). Experimental (24,43) and modeling (23,44) studies are consistent with this, showing a strong correlation between FRQ stability and the period of the clock, with slow FRQ degradation (*frq*^{7}) seen with longer periods whereas fast degradation of FRQ (*frq*^{1}) is seen with shorter periods. Our model simulates periods of *frq*^{1} and *frq*^{7} mutants by changing the FRQ degradation rate constant (Fig. S6), which is consistent with previous results.

The glucose compensation is achieved by balancing the rates of activation between *frq* and *csp-1*

The period of circadian rhythms is relatively insensitive to changes in nutrient conditions. As demonstrated in recent experiments, *Neurospora crassa* showed small changes in period over a wide range of glucose concentrations (16). In contrast, a significantly shorter period was observed in *csp-1*^{ko} compared to WT with increasing glucose levels (16). In the same study, an increased abundance of *wc-1* mRNA and WC-1 were observed in *csp-1*^{ko} compared to WT in high-glucose (2%) but not in low-glucose (0.1%) conditions. On the other hand, a glucose-dependent increased level of CSP-1 was observed in *wc-2*^{ko} (16), which suggested that glucose-induced expression of CSP-1 is independent of WCC. The glucose-dependent repression of *wc-1* transcription by CSP-1 strongly suggests a central role of CSP-1 in a circadian glucose compensation mechanism. This led Sancar et al. (16) to hypothesize that glucose compensation of the circadian period is achieved by balancing increased abundance of WC-1 with the CSP-1-dependent repression of *wc-1* transcription.

To begin with, we simulated the *csp-1*^{ko} strain by setting the rate constant of *csp-1* expression $k_{16} = 0$. We modeled different glucose levels by changing the rate constant of *wc-1* expression, k_7, according to the reported increase in WC-1 protein abundance at high glucose concentrations (16). Our model reproduces the decrease of period as a function of the rate of *wc-1* transcription (k_7) (Fig. 4 *A*). The decrease in period is accompanied by an increase in FRQ_n amplitude (Fig. 4 *B* and see Text S2 in the Supporting Material), whereas the saturation of FRQ_n and $WC\text{-}1_n$ amplitudes (Fig. 4, *B* and *C*) corresponds to the stabilization of the period at ~20 h (Fig. 4 *A*). There exists a narrow region where the period sharply increases with increasing rate constant k_7 (Fig. 4 *A*). This region corresponds to low-amplitude oscillations near Hopf bifurcation (Fig. 4, *B* and *C*) that are easily destroyed by molecular noise (see Fig. S4).

To investigate glucose compensation with our model, we computed the constant period curves in the two-parameter bifurcation plane of the rates of *csp-1* (k_{16}) and *wc-1* (k_7)

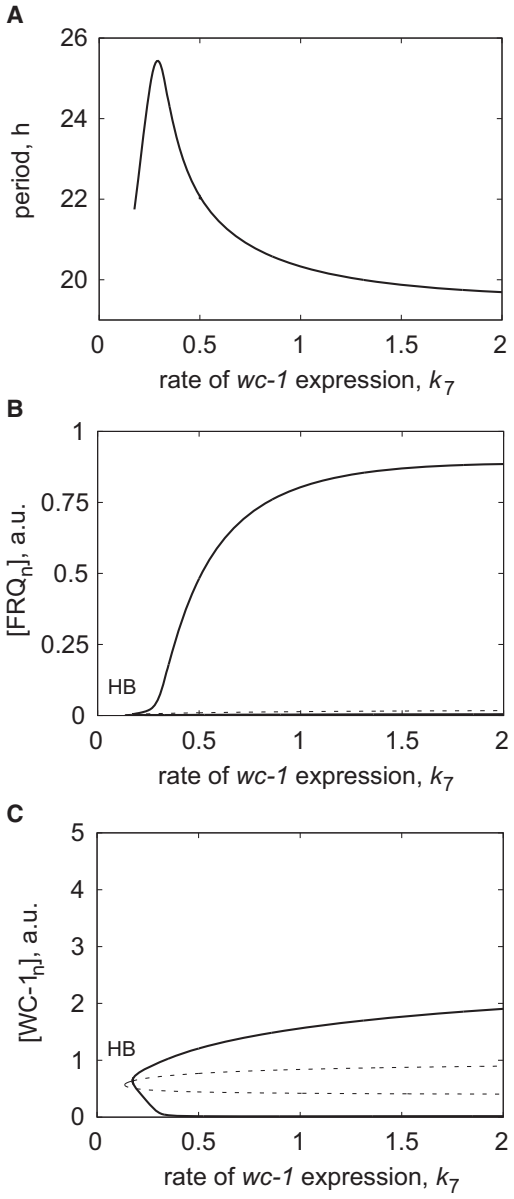

FIGURE 4 Simulated loss of glucose compensation of circadian clock in the *csp-1*^{ko} strain. (*A*) Clock period as a function of parameter k_7, simulating the increase in glucose concentration. One-parameter bifurcation diagrams show the envelopes (maximum and minimum) of (*B*) FRQ_n and (*C*) $WC\text{-}1_n$ oscillations as a function of k_7. Oscillatory region is bounded by supercritical Hopf bifurcation (*HB*) at low values of k_7 and is unbounded at high values of k_7 due to saturation of WC-1 synthesis with respect to *wc-1* mRNA (see Materials and Methods). (*Thick solid curves*) Stable oscillatory solutions; (*thin solid curves*) stable steady states; (*dashed curves*) unstable steady states. The rate of synthesis of *csp-1* mRNA is set to zero ($k_{16} = 0$) for these simulations.

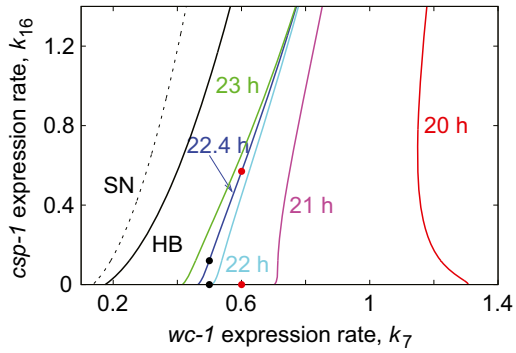

FIGURE 5 Simulated glucose compensation of the clock period in wild-type and its loss in *wc-1*^{ov} mutant. The two-parameter bifurcation diagram in *wc-1* and *csp-1* transcription rate constants k_7 and k_{16}, correspondingly, shows curves of constant period, color-coded. Oscillatory solutions appear from the Hopf bifurcation (*HB*). Parameter sets in low-glucose (*black dots*) and high-glucose (*red dots*) conditions are used for stochastic simulations in the analysis of period robustness against molecular stochasticity. The *csp-1*^{ko} corresponds to the x axis in the diagram ($k_{16} = 0$). The values of the model parameters are as described in Materials and Methods.

transcription (Fig. 5). Our analysis demonstrates that fixed period curves have a remarkably constant positive slope around the wild-type period of ~22.4 h. Hence, simultaneous increase of the above pair of parameters leads to a constant period in the model. The shorter period with an increase of *wc-1* transcription rate as a function of glucose concentration is compensated near the WT period by the longer period with the increase of *csp-1* transcription rate, which results in the repression of *wc-1* expression by the increased amount of CSP-1 (16). Therefore, our model is consistent with the glucose compensation being achieved by balancing the synthesis of *wc-1* and *csp-1*.

Intriguingly, the fixed period curve for a short period ($T = 20$ h) at higher values of k_7 has a negative slope (Fig. 5). Near the period $T = 20$ h ($k_7 = 1.2$), increase of *csp-1* expression rate (k_{16}) results in a shorter period, which is the opposite behavior to when the system is in the wild-type regime ($k_7 = 0.5$). In other words, the balance between *wc-1* and *csp-1* transcription that we observe near the WT period $T = 22.4$ h is no longer present in a different parameter space with a period $T = 20$ h. Therefore, the *wc-1* expression rate has to decrease to maintain constant period, which results in the negative slope of the fixed period curve $T = 20$ h (Fig. 5).

Based on this analysis, our model predicts a loss of glucose compensation in a *wc-1* overexpression mutant (i.e., increased rate of *wc-1* transcription) if we assume that both *csp-1* and *wc-1* synthesis rates increase as a function of glucose concentration in the growth media. To test this hypothesis, we constructed a *wc-1* overexpression strain by transforming an additional *wc-1* gene with its endogenous promoter at the *csp-1* locus into a *Neurospora* strain that contains a *frq-luc* bioluminescence reporter (36). WC-1 protein abundance is increased in the *wc-1*^{ov} strain compared to the wild-type (Fig. 6 *A*). More importantly, the *wc-1*^{ov} strain demonstrates a decrease of period as a function of glucose concentration in both race tube (Fig. 6, *B* and *C*) and *frq-luciferase* bioluminescence assays (Fig. 6 *D*); these data indicate a loss of glucose compensation.

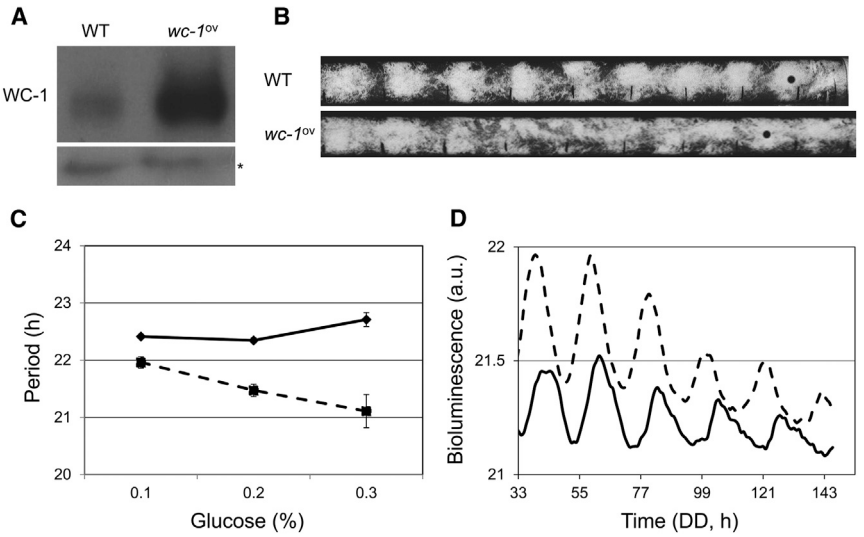

FIGURE 6 Loss of glucose compensation in the *wc-1*^{ov} mutant. (*A*) Western blot shows increased abundance of WC-1 in the *wc-1*^{ov} mutant. Nonspecific bands (*) are shown as a loading control. This is a representative blot from three experiments. (*B*) Representative race tubes of wild-type and the *wc-1*^{ov} mutant grown on a defined agar media (see Materials and Methods) with 0.3% glucose (m/v). (*Small black bars*) Markings of *Neurospora* growth front in every 24 h. (*Black dots* on the race tubes) Period of *wc-1*^{ov} is shorter than the wild-type. (*C*) Graph showing free running periods from wild-type (*solid line*) and *wc-1*^{ov} (*dashed line*) in the media containing different glucose concentrations. The period decreases in *wc-1*^{ov} with increasing glucose concentration in the media. The periods of race tube assay of the wild-type are 22.41 $\pm$ 0.03 h at 0.1% glucose, 22.35 $\pm$ 0.04 h ($n = 6$) at 0.2% glucose, and 22.71 $\pm$ 0.12 h ($n = 6$) at 0.3% glucose. The quantified periods of race tube assay of the *wc-1*^{ov} at different glucose concentrations are 21.96 $\pm$ 0.1 h ($n = 6$) at 0.1% glucose, 21.47 $\pm$ 0.11 h ($n = 6$) at 0.2% glucose, and 21.11 $\pm$ 0.3 h ($n = 5$) at 0.3% glucose. Error bars represent mean $\pm$ SE. (*D*) Graph showing bioluminescence activity from *frq-luciferase* reporter from wild-type (*solid curve*, 21.82 h) and *wc-1*^{ov} (*dashed curve*, 20.87 h). *Neurospora* are grown in the media containing 0.3% glucose (m/v). *wc-1*^{ov} demonstrates shorter period compared to wild-type, which is consistent with (*B*). The figure shows a representative data from three independent experiments.

Analysis of period robustness against molecular stochasticity

It has been shown that the interlocked dual negative feedback loop creates a wider oscillatory domain (21). We wondered if the additional negative feedback loop mediated by CSP-1 enhances the robustness of the system against molecular noise as a function of glucose concentration. To test this hypothesis, we performed stochastic simulations of the clock model to determine the effect of noise on the period of *Neurospora* circadian oscillator in both WT and *csp-1*^{ko} as a function of glucose concentration (i.e., low and high values of k_7 and k_{16}). The period histograms of stochastic simulations in low-glucose conditions (*black dots* in Fig. 5) are plotted in Fig. 7. In the case of a strong noise, the WT parameter set shows larger variation of the periods (Fig. 7 *A*) when compared to the period variation in the case of the *csp-1*^{ko} parameter set (Fig. 7 *B*). In the case of a weak noise, we observed similar behavior except period variation was smaller, as expected for weak noise (Fig. S7, *A* and *B*). Therefore, unexpectedly, *csp-1*^{ko} appears to be slightly more robust than the WT with either strong or weak noise in the system.

We also investigated the effect of noise in the model in high glucose conditions (*red dots* in Fig. 5). Here, similar to low-glucose conditions, the WT had more variation in period compared to *csp-1*^{ko} when strong noise was present (Fig. 7, *C* and *D*). Notably, the WT in high glucose had similar period sensitivity compared to the WT in low glucose (Fig. 7, *C* and *A*), whereas *csp-1*^{ko} in high glucose had less variation in period compared to *csp-1*^{ko} in low glucose (Fig. 7, *D* and *B*). In the case of weak noise, period variation in WT and *csp-1*^{ko} in high glucose resembled the results in the case of strong noise (Fig. S7, *C* and *D*) as well as between high- and low-glucose parameter sets (Fig. S7), but variation of periods was smaller as expected for weak noise. The race tube and bioluminescence data show a robust circadian period with standard errors at ~0.2 h or 10% even in the *csp-1*^{ko}, which is consistent with our simulations (16).

It is important to note that the location of the WT parameter space is closer to the Hopf bifurcation compared to *csp-1*^{ko} parameter space (Fig. 5), because it was previously shown that the proximity of a Hopf bifurcation leads to less robust oscillations against noise (45). Therefore, to make a fair comparison of robustness of *csp-1*^{ko} and WT parameter sets against noise, we performed stochastic simulations of the *csp-1*^{ko} parameter set in very low glucose (Fig. S8) that has a similar distance to Hopf bifurcation as the WT parameter set in low glucose. We observed period variation that was similar to the WT parameter set (Figs. S8 and 7), which indicates that the proximity to the Hopf bifurcation plays a defining role in determining the robustness of circadian oscillations against noise in the *Neurospora* clock.

DISCUSSION

In this article, we constructed a mathematical model of the *Neurospora* circadian clock that incorporates a transcriptional repressor, CSP-1 (15), which resulted in a model with interlocked dual negative feedback loops (Fig. 1). This network topology resembles the mammalian circadian clock model in which REV-ERB-α/β forms a second

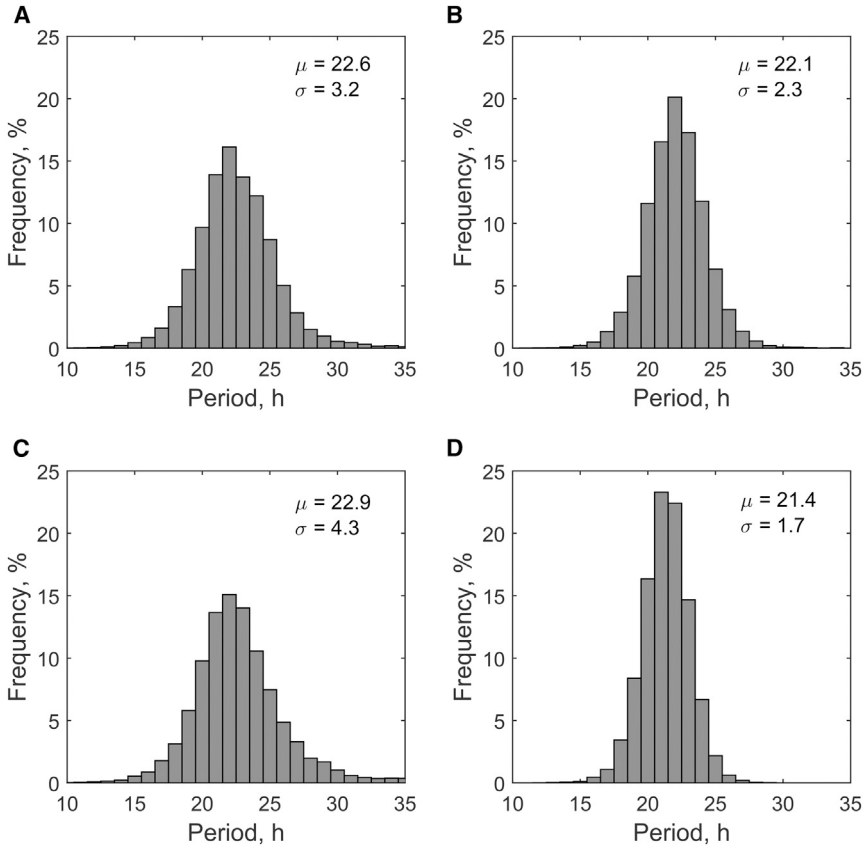

FIGURE 7 Histograms of period distributions obtained by stochastic simulations with strong noise. Period distribution in the presence of strong noise for the WT (*A* and *C*) and *csp-1*^{ko} (*B* and *D*) in low and high glucose, correspondingly. The histograms of periods of 10,000 cycles were computed from 100 simulation runs with 100 successive cycles with the volume factor $\Omega = 100$. The period was determined as the time interval separating two successive peaks of FRQ_c. The mean value (μ) and standard deviation (σ) of the period (in hours) is shown in each histogram. Parameter values are as described in Materials and Methods, except (*B*) $k_{16} = 0$, (*C*) $k_7 = 0.6$, $k_{16} = 0.57$ and (*D*) $k_7 = 0.6$, $k_{16} = 0$.

negative feedback loop inhibiting the circadian clock transcription factor, CLOCK/BMAL1 (21). The model simulates the changes in clock period observed in different overexpression experiments (Fig. 3). Moreover, the model accurately reproduces compensation of clock period across glucose concentrations (Fig. 5) and the loss of this compensation in *csp-1* mutants (Fig. 4 *A*). Glucose compensation in the model is achieved by balancing the rates of *wc-1* and *csp-1* transcription. This balance is lost in the *csp-1* mutant and the period of the clock decreases at high glucose concentration in the media. Our model predicts the loss of glucose compensation in *wc-1*^{ov} mutants (Fig. 5), which indicates that glucose compensation is achieved within a narrow range of parameter space. More importantly, we validate this modeling prediction in experiments (Fig. 6).

Based on our data and the similarities in the regulatory architecture of the fungal and animal circadian clocks (1,46), we hypothesize defective glucose compensation in *Clk* and *Bmal1* overexpression mutant mice. The outcome of this hypothesis will depend on how glucose influences the master clock in the suprachiasmatic nucleus, which coordinates peripheral clocks (47). It has been shown that high-fat diet shifts patterns of mouse food intake and attenuates amplitudes of clock components (48). Similarly, it would be interesting to investigate glucose-dependent changes of phase and amplitude of core circadian clock components in *Neurospora*, and the function of CSP-1 in such responses. Furthermore, it will be critical to investigate the range of glucose compensation and interconnected molecular responses of circadian rhythms and glucose metabolism to determine the glucose metabolism-dependent physiological outcomes.

The robustness of an oscillatory system against molecular noise depends on several factors including the network topology, parameter space, and functions. Recently, several studies investigated the effect of the second negative feedback loop on robustness of the negative feedback oscillatory systems (21,49). Tsai et al. (49) reported no improvement from additional negative feedback in oscillatory range or operational frequency range for simple oscillator models in accord with our findings for the *Neurospora* clock. In contrast, Kim and Forger (21) showed that the additional slow negative feedback loop on the core clock oscillator increases the oscillatory range of the system. More importantly, they also demonstrated that the second negative feedback loop regulates stoichiometric balance of core clock repressors and activators that is critical for sustained oscillations. However, the second negative feedback loop formed by CSP-1 in *Neurospora* is fast relative to the core negative feedback loop (the ratio of *csp-1* mRNA degradation rate to *frq* mRNA degradation rate $\delta \approx 6$). Both the *Neurospora* clock and the model of Tsai et al. (49) include

Hill functions to describe transcription, whereas the model of Kim and Forger (21) uses protein sequestration. A recent study also showed how models behave differently depending on the choice of transcriptional mechanism between protein sequestration and Hill functions (50). Therefore, our study provides further confirmation for the hypothesis that the effect of an additional negative feedback loop on robustness of the system may depend on the mechanism of transcriptional regulation in the model.

Our stochastic simulations revealed that a CSP-1-mediated negative feedback loop does not enhance robustness of the oscillatory system against noise, because the robustness of the circadian oscillator strongly depends on the proximity of the system to the Hopf bifurcation (Figs. 5 and 7), which is in agreement with previous modeling results (21,45). In particular, in the model of Kim and Forger (21), the second negative feedback loop increases the oscillatory range and, thus, increases the distance of the system to the Hopf bifurcation. Moreover, our simulations indicate that the oscillations are quickly lost even in the presence of a weak molecular noise when the system is in immediate vicinity of the Hopf bifurcation (Fig. S4). These modeling results are confirmed by experimental data on *wc-1* overexpression in *wc-1*^{ko} background (6) and on *csp-1* overexpression in *csp-1*^{ko} background (16). These experimental data show weak and fragile conidiation rhythm, reduced amplitude of *frq* bioluminescence, and increased standard errors of circadian periods right after the appearance of oscillations or just before losing their rhythmicity, which strongly suggests loss of robustness of circadian clock against molecular noise near transitions to steady states. In this report, we demonstrate that iterative mathematical modeling and experimental validations advance our detailed understanding of the *Neurospora* circadian system, and continued development of such models will elucidate interconnected molecular responses between the circadian clock and glucose metabolism.

SUPPORTING MATERIAL

Supporting Materials and Methods, 12 figures, and one table are available at http://www.biophysj.org/biophysj/supplemental/S0006-3495(15)00222-2.

ACKNOWLEDGMENTS

We thank H. Kang for her input in our stochastic simulations, and J. Bellman and K. Noh for technical assistance.

This work was supported by Department of Interior grant No. D12AP00005 and the Charles Phelps Taft Research Center, University of Cincinnati.

REFERENCES

1. Dunlap, J. C. 1999. Molecular bases for circadian clocks. *Cell.* 96:271–290.
2. Dunlap, J. C., J. J. Loros, …, R. Lambreghts. 2007. A circadian clock in *Neurospora*: how genes and proteins cooperate to produce a sustained, entrainable, and compensated biological oscillator with a period of about a day. *Cold Spring Harb. Symp. Quant. Biol.* 72:57–68.
3. Baker, C. L., A. N. Kettenbach, …, J. C. Dunlap. 2009. Quantitative proteomics reveals a dynamic interactome and phase-specific phosphorylation in the *Neurospora* circadian clock. *Mol. Cell.* 34:354–363.
4. Cheng, P., Y. Yang, …, Y. Liu. 2001. Coiled-coil domain-mediated FRQ-FRQ interaction is essential for its circadian clock function in *Neurospora*. *EMBO J.* 20:101–108.
5. Crosthwaite, S. K., J. C. Dunlap, and J. J. Loros. 1997. *Neurospora* wc-1 and wc-2: transcription, photoresponses, and the origins of circadian rhythmicity. *Science.* 276:763–769.
6. Cheng, P., Y. Yang, and Y. Liu. 2001. Interlocked feedback loops contribute to the robustness of the *Neurospora* circadian clock. *Proc. Natl. Acad. Sci. USA.* 98:7408–7413.
7. Denault, D. L., J. J. Loros, and J. C. Dunlap. 2001. WC-2 mediates WC-1-FRQ interaction within the PAS protein-linked circadian feedback loop of *Neurospora*. *EMBO J.* 20:109–117.
8. Cheng, P., Q. He, …, Y. Liu. 2005. Regulation of the *Neurospora* circadian clock by an RNA helicase. *Genes Dev.* 19:234–241.
9. Cha, J., S. S. Chang, …, Y. Liu. 2008. Control of WHITE COLLAR localization by phosphorylation is a critical step in the circadian negative feedback process. *EMBO J.* 27:3246–3255.
10. Hong, C. I., P. Ruoff, …, J. C. Dunlap. 2008. Closing the circadian negative feedback loop: FRQ-dependent clearance of WC-1 from the nucleus. *Genes Dev.* 22:3196–3204.
11. Schafmeier, T., A. Diernfellner, …, M. Brunner. 2008. Circadian activity and abundance rhythms of the *Neurospora* clock transcription factor WCC associated with rapid nucleo-cytoplasmic shuttling. *Genes Dev.* 22:3397–3402.
12. Lee, K., J. J. Loros, and J. C. Dunlap. 2000. Interconnected feedback loops in the *Neurospora* circadian system. *Science.* 289:107–110.
13. Shi, M., M. Collett, …, J. C. Dunlap. 2010. FRQ-interacting RNA helicase mediates negative and positive feedback in the *Neurospora* circadian clock. *Genetics.* 184:351–361.
14. Lambreghts, R., M. Shi, …, J. J. Loros. 2009. A high-density single nucleotide polymorphism map for *Neurospora crassa*. *Genetics.* 181:767–781.
15. Sancar, G., C. Sancar, …, M. Brunner. 2011. A global circadian repressor controls antiphasic expression of metabolic genes in *Neurospora*. *Mol. Cell.* 44:687–697.
16. Sancar, G., C. Sancar, and M. Brunner. 2012. Metabolic compensation of the *Neurospora* clock by a glucose-dependent feedback of the circadian repressor CSP1 on the core oscillator. *Genes Dev.* 26:2435–2442.
17. Bugge, A., D. Feng, …, M. A. Lazar. 2012. Rev-erbα and Rev-erbβ coordinately protect the circadian clock and normal metabolic function. *Genes Dev.* 26:657–667.
18. Cho, H., X. Zhao, …, R. M. Evans. 2012. Regulation of circadian behavior and metabolism by REV-ERB-α and REV-ERB-β. *Nature.* 485:123–127.
19. Solt, L. A., Y. Wang, …, T. P. Burris. 2012. Regulation of circadian behavior and metabolism by synthetic REV-ERB agonists. *Nature.* 485:62–68.
20. Schafmeier, T., A. Haase, …, M. Brunner. 2005. Transcriptional feedback of *Neurospora* circadian clock gene by phosphorylation-dependent inactivation of its transcription factor. *Cell.* 122:235–246.
21. Kim, J. K., and D. B. Forger. 2012. A mechanism for robust circadian timekeeping via stoichiometric balance. *Mol. Syst. Biol.* 8:630.
22. Hong, C. I., I. W. Jolma, …, P. Ruoff. 2008. Simulating dark expressions and interactions of frq and wc-1 in the *Neurospora* circadian clock. *Biophys. J.* 94:1221–1232.
23. Ruoff, P., M. Vinsjevik, …, L. Rensing. 1999. The Goodwin oscillator: on the importance of degradation reactions in the circadian clock. *J. Biol. Rhythms.* 14:469–479.

24. Ruoff, P., J. J. Loros, and J. C. Dunlap. 2005. The relationship between FRQ-protein stability and temperature compensation in the *Neurospora* circadian clock. *Proc. Natl. Acad. Sci. USA.* 102:17681–17686.
25. Yu, Y., W. Dong, …, H. B. Schüttler. 2007. A genetic network for the clock of *Neurospora crassa*. *Proc. Natl. Acad. Sci. USA.* 104:2809–2814.
26. Garceau, N. Y., Y. Liu, …, J. C. Dunlap. 1997. Alternative initiation of translation and time-specific phosphorylation yield multiple forms of the essential clock protein FREQUENCY. *Cell.* 89:469–476.
27. Gonze, D., J. Halloy, and A. Goldbeter. 2002. Deterministic versus stochastic models for circadian rhythms. *J. Biol. Phys.* 28:637–653.
28. Gonze, D., W. Abou-Jaoudé, …, J. Halloy. 2011. How molecular should your molecular model be? On the level of molecular detail required to simulate biological networks in systems and synthetic biology. *Methods Enzymol.* 487:171–215.
29. Kim, J. K., K. Josić, and M. R. Bennett. 2014. The validity of quasi-steady-state approximations in discrete stochastic simulations. *Biophys. J.* 107:783–793.
30. Agarwal, A., R. Adams, …, H. Z. Shouval. 2012. On the precision of quasi steady state assumptions in stochastic dynamics. *J. Chem. Phys.* 137:044105.
31. Thomas, P., A. V. Straube, and R. Grima. 2012. The slow-scale linear noise approximation: an accurate, reduced stochastic description of biochemical networks under timescale separation conditions. *BMC Syst. Biol.* 6:39.
32. Kampen, N. G. v. 1992. Stochastic Processes in Physics and Chemistry. North-Holland, Amsterdam, Netherlands.
33. Gillespie, D. T. 1976. General method for numerically simulating stochastic time evolution of coupled chemical-reactions. *J. Comput. Phys.* 22:403–434.
34. Gillespie, D. T. 2007. Stochastic simulation of chemical kinetics. *Annu. Rev. Phys. Chem.* 58:35–55.
35. Chen, C. H., B. S. DeMay, …, J. J. Loros. 2010. Physical interaction between VIVID and white collar complex regulates photoadaptation in *Neurospora*. *Proc. Natl. Acad. Sci. USA.* 107:16715–16720.
36. Gooch, V. D., A. Mehra, …, J. C. Dunlap. 2008. Fully codon-optimized luciferase uncovers novel temperature characteristics of the *Neurospora* clock. *Eukaryot. Cell.* 7:28–37.
37. Hong, C. I., J. Zámborszky, …, A. Csikász-Nagy. 2014. Circadian rhythms synchronize mitosis in *Neurospora crassa*. *Proc. Natl. Acad. Sci. USA.* 111:1397–1402.
38. Dunlap, J. C., and J. J. Loros. 2005. Analysis of circadian rhythms in *Neurospora*: overview of assays and genetic and molecular biological manipulation. *Methods Enzymol.* 393:3–22.
39. Giles, N. H., M. E. Case, …, B. Tyler. 1985. Gene organization and regulation in the QA (quinic acid) gene cluster of *Neurospora crassa*. *Microbiol. Rev.* 49:338–358.
40. Aronson, B. D., K. A. Johnson, …, J. C. Dunlap. 1994. Negative feedback defining a circadian clock: autoregulation of the clock gene frequency. *Science.* 263:1578–1584.
41. Gardner, G. F., and J. F. Feldman. 1981. Temperature compensation of circadian period length in clock mutants of *Neurospora crassa*. *Plant Physiol.* 68:1244–1248.
42. Aronson, B. D., K. A. Johnson, and J. C. Dunlap. 1994. Circadian clock locus frequency: protein encoded by a single open reading frame defines period length and temperature compensation. *Proc. Natl. Acad. Sci. USA.* 91:7683–7687.
43. Liu, Y., J. Loros, and J. C. Dunlap. 2000. Phosphorylation of the *Neurospora* clock protein FREQUENCY determines its degradation rate and strongly influences the period length of the circadian clock. *Proc. Natl. Acad. Sci. USA.* 97:234–239.
44. Ruoff, P., S. Mohsenzadeh, and L. Rensing. 1996. Circadian rhythms and protein turnover: the effect of temperature on the period lengths of clock mutants simulated by the Goodwin oscillator. *Naturwissenschaften.* 83:514–517.
45. Gonze, D., and A. Goldbeter. 2006. Circadian rhythms and molecular noise. *Chaos.* 16:026110.
46. Bell-Pedersen, D., V. M. Cassone, …, M. J. Zoran. 2005. Circadian rhythms from multiple oscillators: lessons from diverse organisms. *Nat. Rev. Genet.* 6:544–556.
47. Stetson, M. H., and M. Watson-Whitmyre. 1976. Nucleus suprachiasmaticus: the biological clock in the hamster? *Science.* 191:197–199.
48. Kohsaka, A., A. D. Laposky, …, J. Bass. 2007. High-fat diet disrupts behavioral and molecular circadian rhythms in mice. *Cell Metab.* 6:414–421.
49. Tsai, T. Y., Y. S. Choi, …, J. E. Ferrell, Jr. 2008. Robust, tunable biological oscillations from interlinked positive and negative feedback loops. *Science.* 321:126–129.
50. Kim, J. K., Z. P. Kilpatrick, …, K. Josić. 2014. Molecular mechanisms that regulate the coupled period of the mammalian circadian clock. *Biophys. J.* 106:2071–2081.